

NEUTRON SCATTERING FROM SOFT HYDROGENOUS MATERIALS

by B.D. Gaulin[†] and J. Katsaras[‡]

[†]Department of Physics and Astronomy, McMaster University, Hamilton, Ontario, L8S 4M1

[‡]National Research Council, Steacie Institute for Molecular Sciences, Neutron Program for Material Research, Chalk River Laboratories, Bldg. 459, Stn 18, Chalk River, Ontario K0J 1J0

ABSTRACT

In non-magnetic materials, neutrons scatter from the nuclei in atoms. This interaction is strong for hydrogen and is very different for protons and deuterons, a fact which makes neutron scattering a technique of choice for the study of soft condensed matter. Such systems, of which polymers, membranes, liquid crystals, and other biomaterials are examples, are always constituted by large amounts of hydrogen, and are often of interest in the presence of a hydrogenous solvent, e.g. water. Unlike x-rays, neutrons are transparent to a variety of materials making them well suited to unusual experimental setups (e.g., samples exposed to high magnetic fields, extremes of temperatures, high pressures, etc.). Their energies, which are of the order of room temperature, make thermal and cold neutrons ideal for materials prone to radiation damage, and inelastic scattering experiments are possible in which energy relevant to their dynamics at temperatures of interest can be transferred to the systems.

The aim of this contribution is to introduce the reader to basic considerations in neutron scattering applied to hydrogenous materials, and to discuss examples of such studies where neutrons have been employed to great advantage in the study of lipid-based, biologically-relevant materials.

NEUTRON SCATTERING

Modern sources of neutrons for use in the study of materials have evolved over a 50 year period to the point where nuclear reactors, optimized for neutron beam research, and pulsed spallation neutron sources possess fluxes fully capable of elucidating much of the structure of macromolecular complexes. [1] In the case of reactor based neutron sources, such as Canada's NRU reactor at Chalk River, the thermal neutron flux is roughly 10^{16} neutrons $\text{cm}^{-2} \text{s}^{-1}$. While compared to present day second and third generation synchrotron x-ray sources, such as the NSLS at Brookhaven and the APS at Argonne, neutron beams are not particularly intense, they are still the preferred probe for a variety of experiments involving soft condensed matter (e.g., [2, 3, 4, 5, 6]).

In non-magnetic materials, neutrons scatter from the nuclei in atoms. Such scattering is nuclei-specific and so is different for different isotopes. Neutrons will also scatter from magnetic moments in matter, both electronic and nuclear in nature. As nuclear moments are completely disordered at all temperatures of interest in this review, such scattering is incoherent. Nuclei are thus characterized by both a coherent and an incoherent neutron scattering length, which quantify the "visibility" of a particular nucleus to neutrons. The atomic form factor is the analogue to the coherent scattering length for x-rays, while there is no x-ray analogue to the incoherent scattering length.

The incoming and scattered neutrons beams, with wave vectors \mathbf{k}_{inc} and \mathbf{k}_{scat} , respectively, impart both momentum $\hbar\mathbf{Q} = \hbar(\mathbf{k}_{inc} - \mathbf{k}_{scat})$ and energy $\hbar\omega = \hbar(k_{inc}^2 - k_{scat}^2)/2m$ to the sample. In the simple case where the sample contains one type of scatterer, labeled with a single coherent and a single incoherent scattering length, the intensity of the scattering in a neutron experiment can be written in terms of a double differential cross section:

$$\frac{d^2\sigma}{d\Omega dE} = \frac{k_{scat}}{k_{inc}} [\sigma_{coh} S_{coh}(\mathbf{Q}, \omega) + \sigma_{incoh} S_{incoh}(\mathbf{Q}, \omega)]$$

where $\sigma_{coh} = 4\pi b_{coh}^2$ and $\sigma_{incoh} = 4\pi b_{incoh}^2$ are, respectively, the coherent and incoherent cross sections of the neutron waves scattered, while b_{coh} and b_{incoh} are the corresponding scattering lengths. Formally, b_{coh} is related to the Fermi

pseudopotential which describes the delta-function interaction between the neutron and the "average" nucleus, while b_{incoh} is a measure of the distribution of pseudopotentials which the neutron may encounter, due to the nuclear spin state or isotope abundance of a particular nucleus.

$S_{coh}(\mathbf{Q}, \omega)$ and $S_{incoh}(\mathbf{Q}, \omega)$ are scattering functions. $S_{coh}(\mathbf{Q}, \omega)$ characterizes the correlations between different parts of the system in time while $S_{incoh}(\mathbf{Q}, \omega)$ characterizes the correlations between the same part of the system at different times. As such $S_{coh}(\mathbf{Q}, \omega)$ contains information on both the structure and dynamics of a given system, while $S_{incoh}(\mathbf{Q}, \omega)$ contains information regarding the dynamics alone.

The scattering ability of neutrons does not depend, as in the case of x-rays, on the atomic number of the element, and neutron cross sections are distributed practically at random (see Table 1) throughout the periodic table. These differences in scattering ability even extend to isotopes of the same element. Therefore, the coherent scattering lengths for certain light (e.g., nitrogen) and heavy (e.g., platinum) elements can be very similar [7]. For soft materials this is significant as they are, for the most part, composed of lighter elements. More importantly for hydrogenous materials is the fact that the scattering lengths of hydrogen, H, and deuterium, D, are vastly different [7]. Neutrons scattered by H atoms are 180° out-of-phase compared to those neutrons scattered by most other atoms including, its isotope deuterium (Table 1). As a result of this phenomenon, the scattering length for hydrogen is negative. It should be noted that for elements occurring in biological systems, hydrogen is about the only negative scatterer of importance [8].

The fact that neutrons have the ability to distinguish between H and D makes isotopic substitution a technique of great importance for the study of hydrogenous materials. This method, commonly known as "contrast variation", was initially developed for light scattering [9] and subsequently modified for x-ray scattering [10]. Using a dilute solution of molecules, small-angle neutron scattering can give detailed information about the configuration of the molecules in solvent due to the contrast in scattering length density between the molecules and the solvent. This contrast between the solvent and the

Table 1 Neutron and atomic scattering lengths of various elements

Element	Scattering Length (10^{-12} cm)	
	Neutrons	X-rays ($\sin \theta = 0$)
H	-0.38	0.28
D	0.65	0.28
C	0.66	1.7
N	0.94	2.0
O	0.58	2.3
P	0.51	4.2
S	0.28	4.5
Cl	0.96	4.8
Ca	0.46	5.6
Mn	-0.36	7.0
Fe	0.95	7.3
Ni	1.0	7.9
Zn	0.56	8.3
Pt	0.95	22.0

solute is easily adjusted over a wide range of solvent scattering length density simply by varying the solvent's H/D ratio, as opposed to methods commonly employed for x-ray scattering [11] which involve the introduction of a variety of impurities (e.g., salt, glucose or sucrose) to the system. In addition, the range of contrast accessible to neutrons is much greater than that accessible to x-rays. This technique can also be applied to high molecular concentrations by selectively deuterating a small fraction of the molecules. We will not report here on any contrast variation studies, however we would like to point out an excellent review by Jacrot [12] which provides many examples of the application of the contrast variation methodology to a variety of biological systems.

The proton incoherent scattering length is very large compared with most nuclei, and this has made incoherent neutron scattering an important technique in the study of the dynamics of hydrogenous materials [13, 14, 15]). Typical cold and thermal neutrons have energies of order 10 meV, and energy transfers as low as 0.1 meV are easily measured. In turn, this implies that inelastic neutron scattering is capable of probing a wide range of motions occurring on time scales from 10^{-9} s to 10^{-13} s, depending on the energy resolution of the spectrometer used [14]. This information is also essential for the refinement of interatomic potentials, which can be used, for example, as input to molecular dynamics calculations [16].

The outline for the remainder of the article will be to first discuss some of the basic structural features of lipid bilayer systems in solvent, and then describe a couple of examples where these features have been successfully examined with neutrons. We move on to give examples of studies in which sophisticated sample environments could be employed in the study of such biosystems, due to the penetrating power of the neutron. We end our brief review with a discussion of another attribute of neutron scattering which may be exploited, which is the ability to easily measure the inelastic scattering cross

section which provides information on dynamic, as opposed to static behaviour.

MODEL MEMBRANE SYSTEMS

Lipids (Fig. 1) are biomolecules which have attracted a great deal of scientific interest for a variety of reasons. One of their attractions is the fact that they are a principal constituent of biological cell membranes with the lipid:protein ratio varying anywhere from 1:4 to 4:1 [17]. As a result of this role within biological membranes, much effort has been expended in understanding the relationship between cellular functions and the lipid matrix [18]. In addition they are lyotropic liquid crystals, which when hydrated, self-assemble into a variety of lamellar (e.g., L_c' , P_{β}' , L_{β}' , L_{α} etc.) (see Fig. 2) [19, 20, 21, 22, 23, 24] and non-lamellar (e.g., cubic, hexagonal and inverted hexagonal) phases (see Fig. 3) [25, 26, 27] and serve as model systems displaying certain low dimensional phase transitions [23, 28, 29].

The lipid molecules are comprised of a polar head group connected via a glycerol backbone to a pair of $n\text{CH}_2\text{-CH}_3$ chains. When emersed in a polar solvent, such as water, the molecules self-organize so as to keep the head group in contact with the solvent and thereby shield the $n\text{CH}_2\text{-CH}_3$ chains from the solvent. This effect, commonly known as the hydrophobic effect, is possibly the single most important factor in organizing simple molecules into complex structural entities [30] as the ones mentioned above and shown schematically in Figures 2 and 3. It is worth mentioning that the hydrophobic effect is mostly the result of the solute (the polar headgroup) bonding strongly with the water, and thus compensating for the disruption of the bonds which had existed in pure water. The attraction of the hydrocarbon chains for each other plays only a minor role [30].

As can be observed from Fig. 1, membrane lipids are relatively small molecules (molecular weight ≈ 800) having a substantial proportion of their weight made up of hydrocarbons. Since water is a prerequisite to the formation of the above-mentioned structures and also for lipids to mimic biological membranes, such lipid/water systems readily lend themselves to neutron scattering studies.

PHASES AND PHASE BEHAVIOUR

In addition to being capable of forming a variety of non-lamellar phases (Fig. 3), lipid/water systems also display a rich variety of lamellar phases as a function of temperature. The lamellar phases shown schematically in Fig. 2 are those exhibited by dipalmitoylphosphatidylcholine (DPPC) in excess water. This particular lipid system is well studied as DPPC is the major lipid constituent in lung surfactant. Both neutron and x-ray diffraction are well suited to elucidating these phases, and the two can be used to great advantage together. We now discuss a recent diffraction study of lamellar DPPC in excess water as a function of temperature.

Small angle neutron scattering (SANS) profiles of multilamellar vesicles of DPPC in excess water, taken by Mason et al. [31], are shown in Fig. 4 as a function of temperature. Diffraction measurements at small angles are required in order to study these structures, as the characteristic periodicities in the multilamellar vesicles are large compared with the wavelengths of the radiation employed in the measurements. This follows from Bragg's law $\lambda = 2d\sin(\theta)$, and the scattering angle θ (2θ is the total angular deflection of a particular scattered neutron) is related to the momentum transfer of the scattering event,

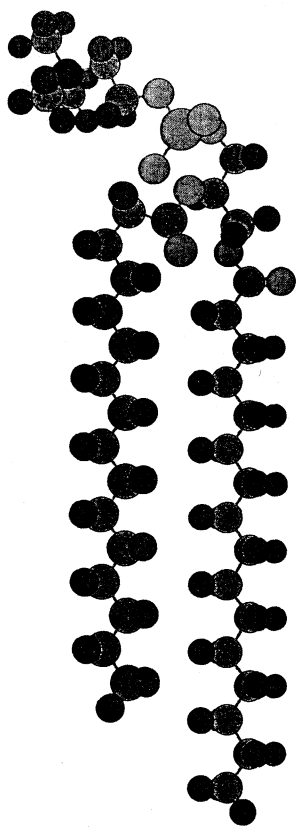


Fig. 1 A schematic representation of a 1,2-dipalmitoyl phosphatidylcholine lipid molecule, specifically dipalmitoyl phosphatidylcholine (DPPC) is shown in silhouette. The polar group (top) is connected via a glycerol backbone to a pair of $n\text{CH}_2\text{-CH}_3$ chains. (see back cover for colour version)

$$Q, \text{ by } Q = \frac{4\pi}{\lambda} \sin(\theta).$$

The three panels of Fig. 4 show the neutron diffraction profiles in each of the three phases which this system displays on cooling near physiological temperatures. The high temperature phase is the smectic-A liquid crystalline L_α phase, the low temperature phase is a crystalline phase, resembling a smectic-C liquid crystalline phase, and known as the "gel" or $L_{\beta'}$ phase. The intermediate phase is the periodically modulated lamellar $P_{\beta'}$ phase [24, 32, 33, 34], first described by Tardieu *et al.* [23]. This $P_{\beta'}$ phase, also known as the "ripple" phase, has recently attracted much attention and despite being vigorously investigated, many outstanding issues remain to be resolved [34]. Clear changes can be seen in the position and width of the diffraction peaks near 0.09 \AA^{-1} in Fig. 4, which signify changes in the lipid bilayer repeat distance, normal to bilayers. In the $P_{\beta'}$ phase an additional peak is observed near 0.05 \AA^{-1} , signifying the appearance of a corrugation or ripple in the bilayers. The $n\text{CH}_2\text{-CH}_3$ chains "melt", that is transform from being rigid to being floppy, at the $P_{\beta'}$ to L_α transition near $T=42^\circ\text{C}$.

This phase behaviour is better appreciated in Fig. 5, which shows the results of many SANS patterns of the kind shown in Fig. 4, now compiled together into a colour contour map of temperature vs momentum transfer, Q , with scattered intensity plotted as colour. The three phases can clearly be observed with the $L_{\beta'}$ to $P_{\beta'}$ transition near $T=33^\circ\text{C}$ and the $P_{\beta'}$ to L_α transition near $T=42^\circ\text{C}$, as already mentioned. As can be seen in Fig. 5, the transition between these phases is

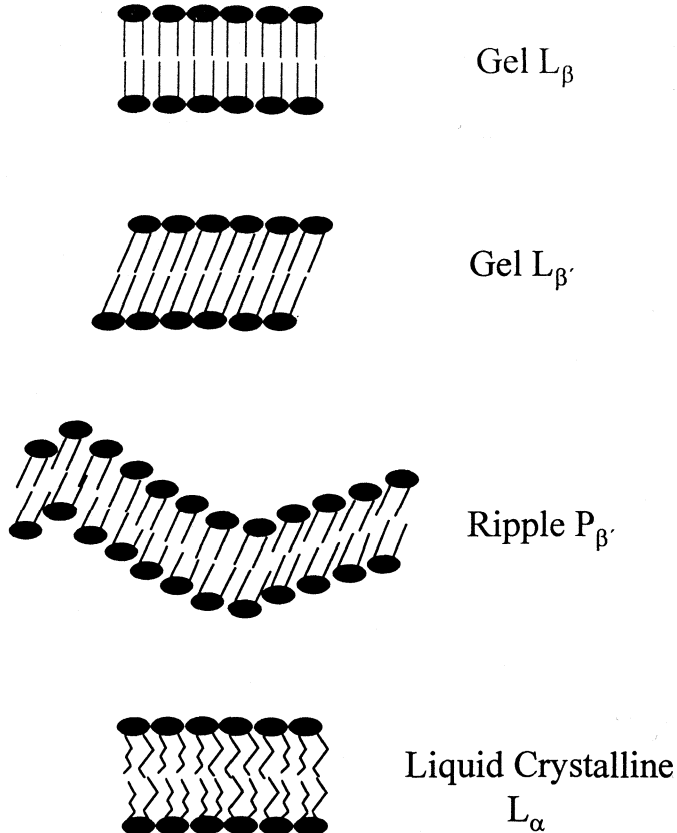


Fig. 2 Schematic representations of various lipid-water phases exhibited by phospholipids having a variety of head groups (e.g., choline, ethanolamine, glycerol, etc.). It should be noted that only phospholipids having the choline head group (e.g., DPPC) can form the rippled $P_{\beta'}$ phase, while phosphatidylethanolamine's (e.g., DPPE) generally have their acyl chains in the non-tilted $L_{\beta'}$ configuration at temperatures below the gel \rightarrow liquid crystalline phase transition.

very abrupt, and these transitions are first order or discontinuous transitions.

Fig. 5 in fact shows two colour contour maps. The top panel shows data taken on warming the sample through the sequence of phases $L_{\beta'}$ to $P_{\beta'}$ to L_α , while the bottom shows data taken on cooling through the L_α to $P_{\beta'}$ to $L_{\beta'}$ sequence. In both cases the temperature and Q region outlined in the white boxes of Fig. 5 were re-examined at higher resolution in order to better understand the nature of the $P_{\beta'}$ phase, and this data is shown as the inset in both panels.

One feature is clear from the contour maps shown in Fig. 5. This is that while the three phases which appear in both warming and cooling are quite similar, history dependencies exist in the scattering within the two "solid" phases, that is the $P_{\beta'}$ and $L_{\beta'}$ phases. The diffraction peak due to the "ripple" periodicity within the $P_{\beta'}$ phase, occurring near $Q=0.05 \text{ \AA}^{-1}$, is much more pronounced on cooling from the L_α phase than if the low temperature $L_{\beta'}$ phase is its precursor. In addition, intense SANS below $Q=0.03 \text{ \AA}^{-1}$ shifts from occurring within the $P_{\beta'}$ phase on warming to occurring within the $L_{\beta'}$ phase on cooling.

While it is not obvious from the data presented in Figs. 4 and 5, it is worth noting that the Bragg-like scattering present in the smectic-A L_α phase of DPPC (top panel of Fig. 4) near

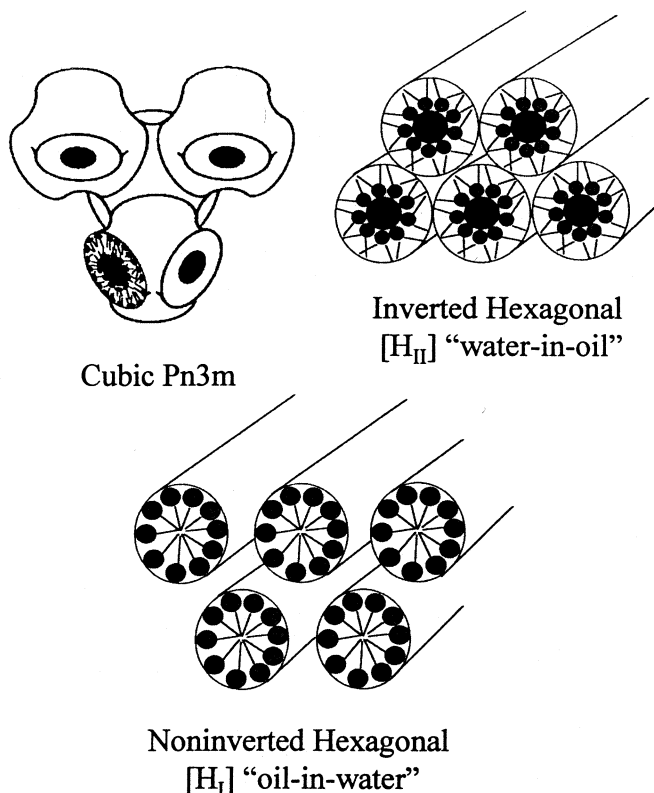


Fig. 3 Several liquid crystalline mesomorphs which can readily be formed by various lipids. For example, under physiological condition dialkylglycerol tetraether lipids from certain bacteria (i.e., pH 3.0, 85 °C) form cubic phases, while phosphatidylethanolamines, monoglucosyldiglycerides and monogalactosyldiglycerides are capable of forming the inverted hexagonal phase. The noninverted hexagonal phase is usually formed by lysolipids or lipids having only one acyl chain. It should be noted that under extreme conditions (e.g., high temperatures and/or hydration), lipids can be induced to form a variety of mesophases.

$Q=0.09 \text{ \AA}^{-1}$ is known to be indicative of "quasi-long range order" [35]. These Bragg-like features are power law singularities in Q as opposed to the delta-functions which characterize Bragg scattering features exhibited by conventional three dimensional solid structures.

Complementary small angle x-ray scattering measurements have also been performed by Mason et al [31]. on the same system over similar ranges of temperature and Q . Together with the SANS measurements discussed above, these authors have concluded that the nature of the corrugated bilayer surfaces is fundamentally different depending on whether the $P_{\beta'}$ phase is entered from above or below in temperature. When entered from the smectic-A L_{α} phase the corrugated lamellae form a well developed long wavelength ripple with a highly monoclinic unit cell (meaning that the peaks and troughs of the ripples on neighbouring lamellae do not lie directly above and below each other, but rather individual rippled lamellae are substantially phase shifted relative to their neighbours). In contrast when the $P_{\beta'}$ phase is entered from the $L_{\beta'}$ phase, that is from below in temperature, the result is a less ordered ripple with a wavelength roughly half of that obtained in the $P_{\beta'}$ phase on cooling.

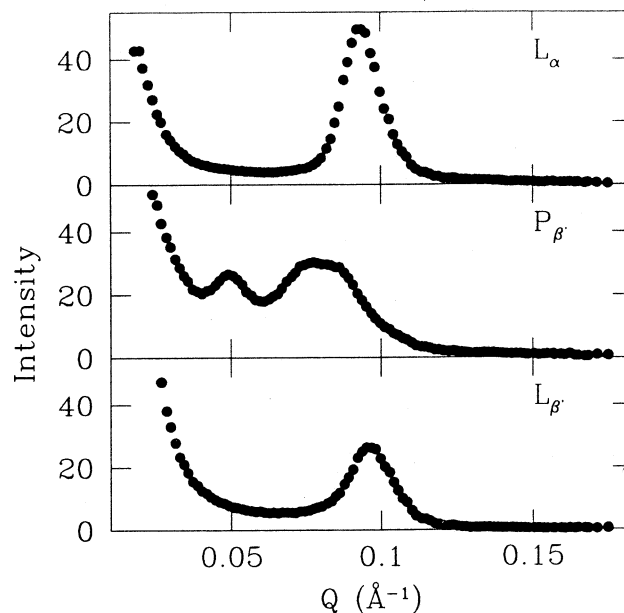


Fig. 4 SANS profiles from DPPC [31] in each of its three phases near physiological temperatures. Scans of this form make up the colour contour scattering map shown in Figure 5.

REPULSION FORCE MEASUREMENTS IN $L_{\beta'}$ PHASE MULTIBILAYERS

Biological structures, such as cells, are separated from each other by an aqueous phase. The interactions which occur between membrane surfaces in solvent are of biological relevance. At small bilayer-bilayer separations ($\leq 20 \text{ \AA}$) the basic forces are the van der Waals attractive forces, and repulsive forces arising from either entropic fluctuations [36] or direct hydration [37], all of which play an important role in cell-cell interactions, protein assembly and cell fusion.

There are both theoretical [38] and experimental [37, 39] studies which demonstrate the presence of a strong repulsive force commonly known as the "hydration force" and which is believed to be the result of lipid molecules perturbing the water structure near the lipid/water interface [40]. However, in recent years a completely different explanation has been put forward which argues that the repulsive forces between dynamic interfaces, such as lipid bilayers, are primarily the result of conformational entropic fluctuations [36, 41, 42]. Experimentally, it has been shown that in fluid sodium dodecyl sulfate bilayers, the repulsive force is dominated at large intermembrane distances ($38 \text{ \AA} \leq d \leq 163 \text{ \AA}$) by entropic steric undulatory forces [43] previously described by Helfrich [44].

X-ray diffraction has been commonly used [37, 39, 41] in the construction of pressure-distance curves used to differentiate between the various proposals for repulsive forces [45], however neutron diffraction can also give important information. The distances between structural units in a multilamellar assembly can be determined by a crystallographic analysis of the diffraction features. As many Bragg-like reflections as possible are measured, and these are related to the Fourier transform of the electron (x-rays) or coherent scattering length (neutron) densities in the multilayers. If the Bragg reflections are chosen to be those in which Q is normal to the bilayers, then a one

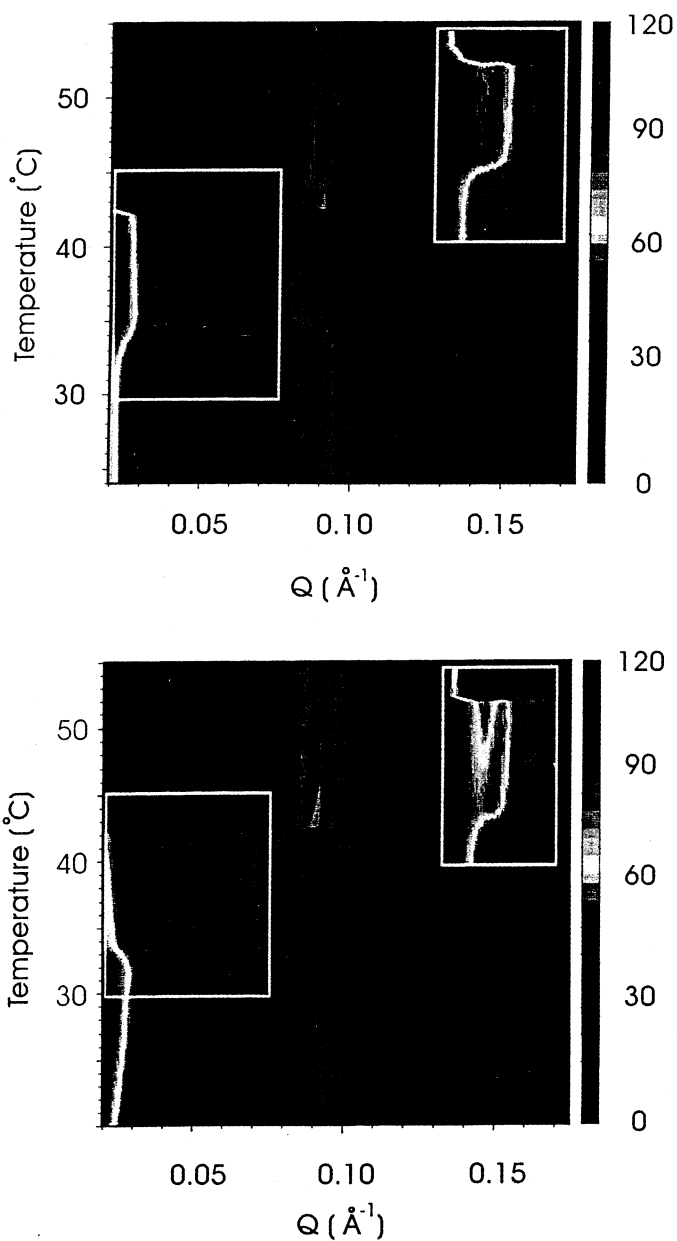


Fig. 5 A colour contour plot made up from many SANS profiles of the form shown in Fig. 4. The top panel shows data taken on warming through the sequence of phases $L_{\beta'}$ to $P_{\beta'}$ to L_{α} , while the bottom panel shows data taken on cooling through the sequence of phases L_{α} to $P_{\beta'}$ to $L_{\beta'}$. Clear history dependencies are seen in the two "solid" phases, $P_{\beta'}$ and $L_{\beta'}$, which are interpreted as coherent (on cooling) and incoherent (on warming) ordering of the corrugated lamellae associated with the $P_{\beta'}$ phase.

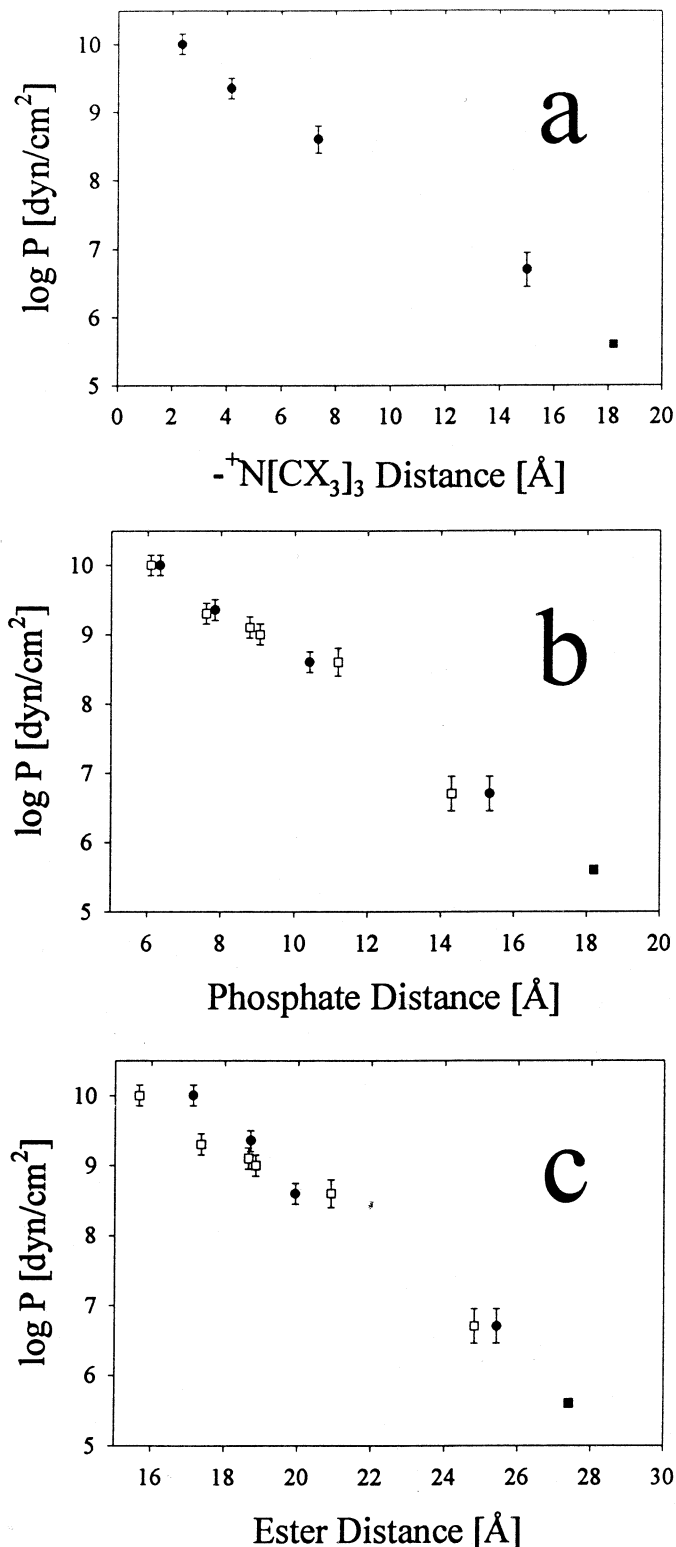


Fig. 6 The logarithm of applied pressure ($\log P$) vs distance between various groups along the bilayer is shown. Separations between adjacent (a) *tert*-methylamine, (b) phosphate and (c) ester groups obtained using a variety of humidities. The distances represented by filled circles were obtained from neutron measurements, open squares from x-ray diffraction measurements and the filled squares from a previous x-ray datum of excess water DPPC multibilayers (please see Ref. [46]).

dimensional scattering density profile, along the bilayer normal, can be constructed, and from these the distance between structural units can be picked off. Complementary neutron and x-ray analysis in this manner yields two independent scattering density profiles, which gives much more structural information and also serves as a consistency check.

Osmotic pressure can be controlled via the use of a variety of saturated salt solutions giving rise to sample environments having a known relative humidity. A plot of the log of the osmotic pressure vs bilayer separation should yield very different results for the various predicted types of forces. For the hydration force, an exponential dependence of the osmotic pressure on bilayer separation is predicted by the order parameter model of the repulsive hydration pressure first proposed by Marcelja and Radić [40]. On the other hand, for undulatory steric repulsion of the type predicted by Helfrich, a power law dependence is expected [44]. Finally, a discontinuity in the pressure-distance curve at very small interbilayer spacings (e.g., 3 - 5 Å) is the signature of head group collisions and molecular protrusions [39, 42].

Using data obtained from a combination of neutron and x-ray diffraction measurements, pressure-distance curves were constructed from calculated one-dimensional neutron and x-ray scattering density profiles for three distinct regions of DPPC bilayers in the gel L_{β} phase [46]. This data, presented in Fig. 6, is consistent with the model proposed by Marcelja and Radić [40] in which an exponential dependence of the pressure-distance curve is predicted. It is important to note, that the separations between the *tert*-methylamine groups at various humidity levels (Fig. 6a) could only have been obtained from difference neutron scattering profiles of DPPC molecules containing either protonated or deuterated *tert*-methylamine groups [$(^+N(CD_3)_3)$ - $(^+N(CH_3)_3)$], since x-rays scatter rather poorly from the *tert*-methylamine group of atoms.

THE STUDY OF MATERIALS IN SOPHISTICATED SAMPLE ENVIRONMENTS

LARGE MAGNETIC FIELDS

The structural information accessible from diffraction experiments is greatly enhanced if the data collected is obtained using a well-aligned sample (e.g., [19, 24, 28]). Although there are a variety of methods which have been developed to align hydrogenous materials (e.g., [47, 48, 49]), one method is alignment in large magnetic fields (e.g., ≥ 1.5 T) of molecular assemblies exhibiting sufficient diamagnetic anisotropy [50, 51, 52, 53]. X-ray diffraction has been used to study magnetically aligned samples (e.g., [52, 54]), however the technique is limited in its use of small permanent magnet assemblies with gap spacings < 1 mm. These are capable of producing uniform magnetic fields up to a maximum of 2 T [55]. This limitation in magnetic field and sample volume is due to the relatively small penetration depth for ~ 8 keV x-rays in most materials which would be used in such sophisticated sample environments. This factor can preclude the investigation of certain systems such as red blood cells, which happen to align in magnetic fields of ≥ 6 T [50]. In contrast, neutrons penetrate relatively deeply into most materials, with characteristic penetration depths of the order of 1 cm. As a result of the relative transparency of the sample environment neutron diffraction experiments can be carried out with large superconducting solenoids (often with split coils) and have been carried-out at magnetic fields as high as 42 T [56].

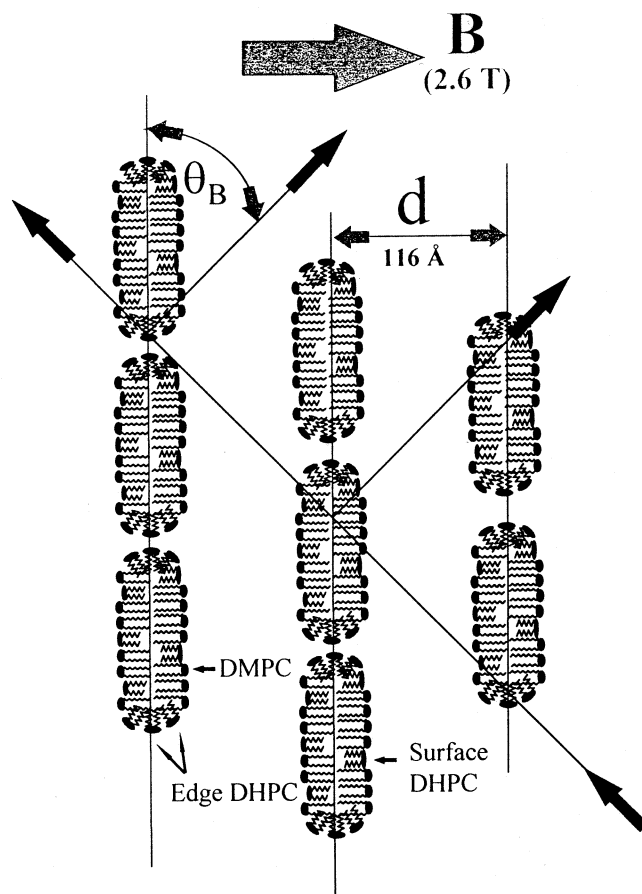


Fig. 7 A schematic diagram of the diffraction geometry used to study the magnetically alignable DMPC/DHPC/water system doped with Tm^{3+} ions. The bilayers are in the L_{α} phase and when aligned using a 2.6 T magnetic field exhibit a mosaic spread of $\leq 1.0^{\circ}$.

Recent neutron diffraction experiments in the presence of magnetic fields of up to 2.6 T, have shown that amphiphilic assemblies (Fig. 7) composed of phosphorylcholine lipids [57] undergo a rare nematic (1D ordering) \rightarrow smectic (2D ordering) transition (Fig. 8) when doped with the paramagnetic lanthanide ion Tm^{3+} [2]. Previously, deuterium quadrupole echo nuclear magnetic resonance (NMR) had shown that the addition of Tm^{3+} , to these so-called "bicelles", resulted in the bicelles having their bilayer normals parallel to the magnetic field (Fig. 7) [58] rather than perpendicular to the field direction, as they were prior to the addition of the paramagnetic ions [57, 58, 59, 60]. The neutron diffraction data from this system in both the absence and presence of Tm^{3+} ions at a constant magnetic field of 2.6 T are shown in Fig. 8. Sharp diffraction features (Fig. 8a) consistent with the lamellar structure are present in the Tm^{3+} doped sample, but disappear in the absence of Tm^{3+} (Fig. 8b), leaving only a shoulder in the scattering at $\sim 0.06 \text{ \AA}^{-1}$, characteristic of nematic order.

In addition to the nematic \rightarrow smectic transition, the neutron data revealed that at 2.6 T the bilayer stacks were highly aligned [$\leq 1.0^{\circ}$ mosaic, Fig 8(a) inset] having an out-of-plane correlation length of $\approx 1400 \text{ \AA}$ [2]. It has also been shown using ^{13}C NMR, that the bicelle system can be used as a substrate to align a variety of polypeptides and proteins independent of the macromolecule's intrinsic magnetic properties [60].

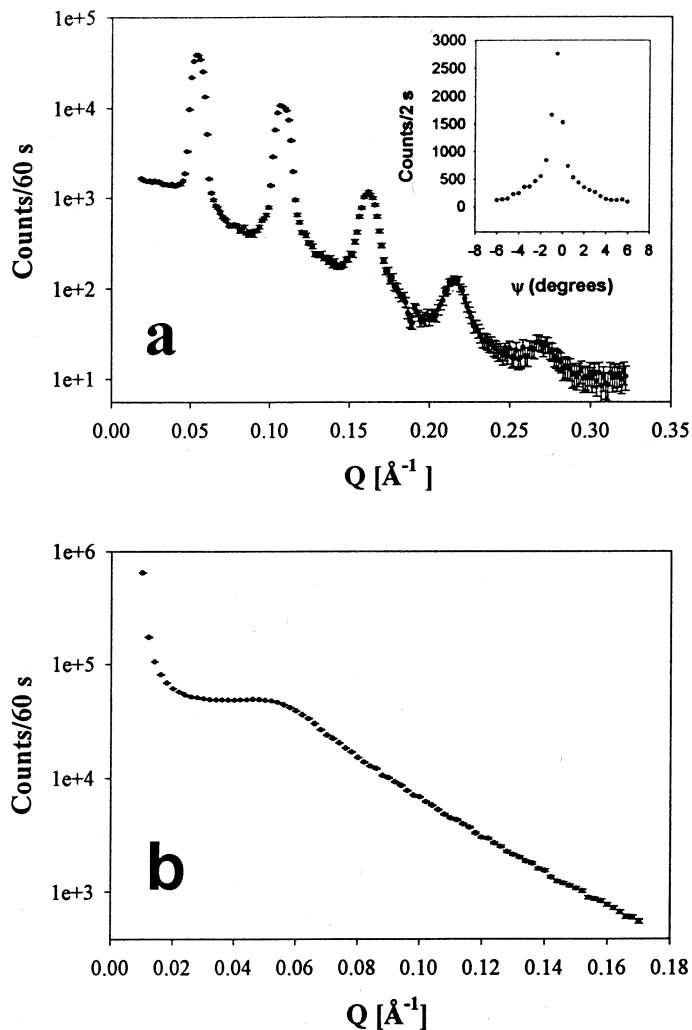


Fig. 8 (a) Diffraction pattern from the DMPC/DHPC unilamellar bilayer stack system doped with Tm^{3+} at 315 K and $B = 2.6$ T. The FWHM of the Bragg peaks increases linearly with increasing scattering angle indicative of a 2D "fluid" system. At $2\theta_B = 0$ the incident beam was orthogonal to the applied magnetic field. (b) Q scan of the dimyristoyl phosphorylcholine/dihexanoyl phosphorylcholine (DMPC/DHPC) system in the absence of Tm^{3+} at a temperature of 315 ± 1 K and a magnetic field of 2.6 T. The diffraction geometry was such that at $2\theta_B = 0$ the incident beam was parallel to the applied magnetic field.

Although other systems have previously been developed to act as alignable substrates (e.g., [51, 61]), the bicelle system is the first of its type, composed solely of biologically relevant molecules.

HIGH-PRESSURE EXPERIMENTS

Although many materials are essentially transparent to neutrons, neutron diffraction experiments at high hydrostatic pressure were, until recently, confined to pressures below 3 GPa as a result of the relatively large sample volume required. Due to this limitation, x-rays, with their high brilliance sources, have been the tool of choice for much high-pressure materials research. For example, some x-ray experiments have employed pressures of up to 300 GPa [62]. A newly-developed high pressure neutron scattering cell has greatly improved the

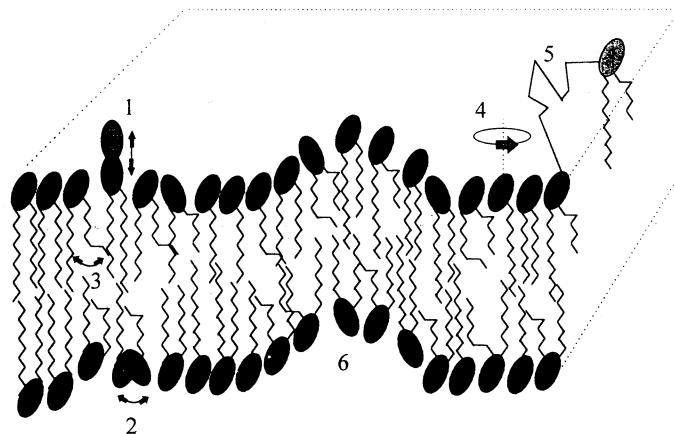


Fig. 9 Various types of motions present in a fluid bilayer are schematically shown: 1) Individual lipid molecule out-of-plane or vertical vibrational motion.; 2) Flip-flop motion of lipid head group; 3) Chain defect motions; 4) Rotational diffusion of lipid molecules about their long axis; 5) In-plane or lateral diffusion of lipid molecules; 6) Collective undulations of the lipid bilayer.

capabilities for neutron experiments under high pressure, and experiments can now be performed at pressures exceeding 30 GPa with sample volumes of the order of 30 - 100 mm^3 [63, 64]. Even so, for full structural refinements the maximum pressure lies in the range of 10 - 20 GPa. While the maximum applied pressure is less than that which can be obtained in similar x-ray diffraction measurements, such high pressure neutron experiments can exploit the same sensitivity to low atomic number elements, and in particular hydrogen, which is so important in the study of soft materials [3, 63, 64, 65, 66, 67].

INELASTIC NEUTRON SCATTERING

Phospholipid assemblies exhibit dynamical behaviour (Fig. 9) with correlation times ranging from 10^{-12} s associated with the motion of chain defects to 1 s corresponding to collective excitations of the bilayer [14] and many of these motions are essential for the function of biological membranes [44, 45, 68, 69, 70]. The inelastic scattering associated with many of these motions occurs over a range of energies at any one wavevector. Often the intensity of this inelastic scattering increases with decreasing energy, such that it peaks at the elastic position but has an intrinsic width in energy (in contrast to true elastic scattering which is a delta-function in energy). This type of inelastic scattering is commonly referred to as quasi-elastic scattering to distinguish it from the inelastic scattering associated with a neutron creating or destroying normal modes (of the lattice for example, a phonon) which occurs at well-defined energies for any one particular wavevector.

Incoherent quasi-elastic neutron scattering (IQENS) is capable of probing dynamics on a wide range of time scales that are difficult to access using other spectroscopic techniques. Hydrogen possesses a much higher incoherent neutron scattering

length than deuterium, thus the dynamics of a subsection of the overall structure can be studied with partial deuteration of the molecules to screen-out the local dynamics of the deuterated portion of the molecule. In addition, use of an aligned sample allows directional dependencies in the dynamics to be studied by selecting the direction of momentum transfer with respect to the bilayer normal [14, 71]. Experiments of this sort have been carried-out using aligned multibilayers of DPPC having perdeuterated hydrocarbon chains.

Several different types of inelastic neutron scattering spectrometers have been built which are optimized for measuring the inelastic scattering over different ranges of Q and $\hbar\omega$, and with different resolution [1]. Measurements have been performed using a time-of-flight spectrometer which resolved dynamics occurring on the time scale between 10^{-11} and 10^{-13} s [14]. In this time regime, the membrane dynamics are dominated by the motion of defects along the $n\text{CH}_2\text{-CH}_3$ chains. These defects can be thought of as antiphase domain walls in the $n\text{CH}_2$ part of the chain, and are known as *gauche-trans* isomerizations. It was found by König *et al.* that in DPPC the number of *gauche-trans* isomerizations increased continuously as a function of increasing temperature (from 2 °C to 70 °C) while the mean displacement of protons from the lipid molecule's cylindrical axis grew from ≈ 0.6 Å near the glycerol backbone to ≈ 7 Å near the centre of the bilayer. This picture is consistent with the probability of occurrence of such chain defects increasing towards the end of the hydrocarbon chain [72].

Inelastic measurements have also been carried out with a backscattering spectrometer, which is sensitive to motions in the time regime of 10^{-9} to 10^{-11} s. These measurements investigated characteristic diffusion times for the lipid molecules within the smectic A, L_α , phase, and concluded [14] that the long-range lateral diffusion coefficient was of the order of 9.7×10^{-8} cm²/s and in good agreement with fluorescence photobleaching recovery measurements. In addition, the out-of-plane motion was characterized by an amplitude of 2-3 Å. In a separate IQENS study, the rotational diffusion coefficient of DPPC multibilayers in the L_α phase and under excess water conditions was found to be 2×10^{-9} s⁻¹ while a lateral diffusion coefficient of 1.8×10^{-7} cm²s⁻¹ was obtained [71].

CONCLUSIONS

We have discussed the application of neutron scattering to selected problems in soft hydrogenous materials. This review is necessarily brief, but we hope it gives a proper flavour for the type and quality of structural and dynamical information which is obtainable with neutron techniques. To summarize, neutrons possess three principal attributes which, when used effectively can make neutron scattering an extremely powerful scattering probe of materials in general and soft materials in particular. These are:

- The sensitivity of neutrons to hydrogen, and the contrast between hydrogen and deuterium coherent neutron scattering lengths which means that contrast variation techniques can be exploited to highlight substructure.
- Neutrons possess a spin $\frac{1}{2}$ magnetic moment and couple to magnetic moments in matter. This includes nuclear moments giving rise to incoherent inelastic scattering from hydrogen which can give unique dynamical information.
- Neutron penetration depths in most materials are ~ 1 cm, and therefore neutrons can get into and out of sophisticated sample environments made from machined metals.

ACKNOWLEDGMENTS

It is a pleasure to acknowledge our collaborators with whom much of the work described in this review was performed: R.M. Eppard, K.R. Jeffrey, J.S. Lin, P.C. Mason, R.S. Prosser, V.A. Raghunathan and G.D. Wignall.

GENERAL REFERENCES

- B. Jacrot. "The study of biological structures by neutron scattering from solution". *Rep. Prog. Phys.* 1976, 39: 911-953.
- A.E. Blaurock. "Evidence of bilayer structure and of membrane interactions from x-ray diffraction analysis". *Biochim. Biophys. Acta* 1982, 650: 167-207.
- N.P. Franks and W.R. Lieb. "X-ray and neutron diffraction studies of lipid bilayers". In "Liposomes: From physical structure to therapeutic applications". Ed. C.G. Knight. Elsevier/North Holland Biomedical Press, 1981 pp 242-272.
- J. Katsaras. "X-ray diffraction studies of oriented lipid bilayers". *Biochem. Cell Biol.* 1995, 73: 209-218.
- K. Skold and D.L. Price (editors). "Neutron Scattering", *Methods of Experimental Physics*, Vol. 23, Parts A,B, and C, Academic Press, Inc., 1986.

REFERENCES

- [1] For general references on neutron scattering see: **Neutron Scattering**, *Methods of Experimental Physics*, Vol. 23, Parts A, B, and C, K. Skold and D.L. Price (eds.), Academic Press, Inc., (1986).
- [2] J. Katsaras, R.L. Donaberger, I.P. Swainson, D.C. Tennant, Z. Tun, R.R. Vold and R.S. Prosser, *Phys. Rev. Lett.* **78**, 899 (1997).
- [3] G. Strauß, A. Bassen, H. Zweier, H. Bertagnolli, K. Tödheide, A.K. Soper and J. Turner, *Phys. Rev. E* **53**, 3505 (1996).
- [4] N. Torikai, Y. Matsushita, I. Noda, A. Karim, S.K. Satija and C.C. Han, *Physica B* **213&214**, 694 (1995).
- [5] B. Farago, M. Monkenbusch, K.D. Goecking, D. Richter and J.S. Huang, *Physica B* **213&214**, 712 (1995).
- [6] M. Kakitani, T. Imae and M. Furusaka, *J. Phys. Chem.* **99**, 16018 (1995).
- [7] V.F. Sears, *Neutron News*, **3**, 26 (1992).
- [8] B.P. Schoenborn, in **Methods in Enzymology** Vol 114, Academic Press, Inc., 1985 pp. 510-529, edited by H.W. Wyckoff, C.H.W. Hirs, and S.N. Timasheff.
- [9] M. Benoit and C. Wippler, *J. Chim. Phys.* **57**, 524 (1960).
- [10] H.B. Stuhrmann and R.G. Kriste, *Z. Phys. Chem.* **46**, 247 (1965).
- [11] K. Ibel and H.B. Stuhrmann, *J. Mol. Biol.* **93**, 255 (1975).
- [12] B. Jacrot, *Rep. Prog. Phys.* **39**, 911 (1976).
- [13] S. König, E. Sackmann, D. Richter, R. Zorn, C. Carlile and T.M. Bayerl, *J. Chem. Phys.* **100**, 3307 (1994).
- [14] S. König, W. Pfeiffer, T. Bayerl, D. Richter and E. Sackmann, *J. Phys. II France*, **2**, 1589 (1992).
- [15] P. Martel and H. Lin, *J. Biol. Phys.* **17**, 137 (1989).
- [16] P. Martel, *Prog. Biophys. Molec. Biol.* **57**, 129 (1992).

- [17] L. Stryer, *Biochemistry*, W.H. Freeman and Co., San Francisco (1981).
- [18] P. Yeagle (Ed), *The Structure of Biological Membranes*, CRC Press, Inc., (1992).
- [19] V.A. Raghunathan and J. Katsaras, *Phys. Rev. Lett.* **74**, 4456 (1995).
- [20] M.C. Weiner and S.H. White, *Biophys. J.* **61**, 434 (1992).
- [21] J. Katsaras, *J. Phys. Chem.* **99**, 4141 (1995).
- [22] J. Katsaras, V.A. Raghunathan, E.J. Dufourc and J. Dufourcq, *Biochemistry* **34**, 4685 (1995).
- [23] A. Tardieu, V. Luzzati and F.C. Reman, *J. Mol. Biol.* **75**, 711 (1973).
- [24] J. Katsaras and V.A. Raghunathan, *Phys. Rev. Lett.* **74**, 2022 (1995).
- [25] J. Katsaras, K.R. Jeffrey, D.S.-C. Yang and R.M. Epand, *Biochemistry* **32**, 10700 (1993).
- [26] D.C. Turner, S.M. Gruner and J.S. Huang, *Biochemistry* **31**, 1356 (1992).
- [27] S.M. Gruner, P.R. Cullis, M.J. Hope and C.P.S. Tilcock, *Ann. Rev. Biophys. Chem.* **14**, 211 (1985).
- [28] G.S. Smith, E.B. Sirota, C.R. Safinya and N.A. Clark, *Phys. Rev. Lett.* **60**, 813 (1988).
- [29] J.L. Ranck, *Chem. Phys. Lipids* **32**, 251 (1983).
- [30] C. Tanford, *The Hydrophobic Effect: Formation of Micelles and Biological Membranes*, John Wiley and Sons, Inc., (1980).
- [31] P.C. Mason, B.D. Gaulin, R.M. Epand, G.D. Wignall and J.S. Lin, (to be published).
- [32] J.T. Woodward and J.A. Zasadzinski, *Phys. Rev. E* **53**, 3044 (1996).
- [33] W.-J. Sun, S. Tristram-Nagle, R.M. Suter and J.F. Nagle, *Proc. Natl. Acad. Sci. USA* **93**, 7008 (1996).
- [34] T.C. Lubensky and F.C. MacKintosh, *Phys. Rev. Lett.* **71**, 1565 (1993).
- [35] P.M. Chaikin and T.C. Lubensky, **Principles of Condensed Matter Physics**, Chap. 2, Cambridge University Press, (1995).
- [36] J.N. Israelachvili and H. Wennerström, *J. Phys. Chem.* **96**, 520 (1992).
- [37] R.P. Rand and V.A. Parsegian, *Biochim. Biophys. Acta* **988**, 351 (1989).
- [38] R. Lipowsky and S. Grotehans, *Europhys. Lett.* **23**, 599 (1993).
- [39] T.J. McIntosh and S.A. Simon, *Biochemistry* **32**, 8374 (1993).
- [40] S. Marcelja and N. Radić, *Chem. Phys. Lett.* **42**, 129 (1976).
- [41] S.H. White and G.I. King, *Proc. Natl. Acad. Sci. USA* **82**, 6532 (1985).
- [42] M.K. Granfeldt and S.J. Miklavic, *J. Phys. Chem.* **95**, 6351 (1991).
- [43] C.R. Safinya, D. Roux, G.S. Smith, S.K. Sinha, P. Dimon, N.A. Clark and A.M. Bellocq, *Phys. Rev. Lett.* **57**, 2718 (1986).
- [44] W. Helfrich, *Z. Naturforsch.* **33 A**, 305 (1978).
- [45] J.N. Israelachvili and H. Wennerström, *Langmuir* **6**, 873 (1990).
- [46] J. Katsaras and K.R. Jeffrey, *Europhys. Lett.* **38**, 43 (1997).
- [47] J.C. Wittmann and P. Smith, *Science* **352**, 414 (1991).
- [48] N.A. Clark, K.J. Rothschild, D.A. Luippold and B.A. Simon, *Biophys. J.* **31**, 65 (1980).
- [49] J. Torbet, and M.H.F. Wilkins, *J. Theor. Biol.* **62**, 447 (1976).
- [50] T. Takeuchi, T. Mizuno, T. Higashi, A. Yamagishi and M. Date, *Physica B* **201**, 601 (1994).
- [51] J.B. Hayter, R. Pynn, S. Charles, A.T. Skjeltorp, J. Trehwella, G. Stubbs and P. Timmins, *Phys. Rev. Lett.* **62**, 1667 (1989).
- [52] M.J. Glucksman, R.D. Hay and L. Makowski, *Science* **14**, 1273 (1986).
- [53] I. Sakurai, Y. Kawamura, A. Ikegami and S. Iwayanagi, *Proc. Natl. Acad. Sci. USA* **77**, 7232 (1980).
- [54] B.J. Hare, J.H. Prestegard and D.M. Engelman, *Biophys. J.* **69**, 1891 (1995).
- [55] R. Oldenbourg and W.C. Phillips, *Rev. Sci. Instrum.* **57**, 2362 (1986).
- [56] R. Gersdorf, L.W. Roeland and W.C.M. Mattens, *IEEE Trans. Mag.* **24**, 1052 (1988).
- [57] C.R. Sanders II and J.P. Schwonek, *Biochemistry* **31**, 8898 (1992).
- [58] R.S. Prosser, S.A. Hunt, J.A. DiNatale and R.R. Vold, *J. Am. Chem. Soc.* **118**, 269 (1996).
- [59] C.R. Sanders II and J.H. Prestegard, *Biophys. J.* **58**, 447 (1990).
- [60] C.R. Sanders II and G.C. Landis, *Biochemistry* **34**, 4030 (1995).
- [61] T. Sosnick, S. Charles, G. Stubbs, P. Yau, E.M. Bradbury, P. Timmins and J. Trehwella, *Biophys. J.* **60**, 1178 (1991).
- [62] U. Benedict, C. Dufour, S. Heathman, T. Lebihan, J.S. Olsen, L. Gerward, R.G. Haire, Y.K. Vohra and G.L. Gu, *High Pressure Research* **14**, 393 (1996).
- [63] J.M. Besson and R.J. Nelmes, *Physica B* **213 & 214**, 31 (1995).
- [64] R.J. Nelmes, J.S. Loveday, R.M. Wilson, J.M. Besson, S. Klotz, G. Hamel, and S. Hull, *Am. Cryst. Assoc.* **29**, 19 (1993).
- [65] S. Klotz, J.M. Besson, M. Brasen, K. Karch, F. Bechstedt, D. Strauch and P. Pavone, *Phys. Status Solidi B*, **198**, 105 (1996).
- [66] H. Bertagnolli and K. Todheide, *J. Phys-Condensed Matter* **8**, 9293 (1996).
- [67] S. Klotz, J.M. Besson, G. Hamel, R.J. Nelmes, J.S. Lovejoy and W.G. Marshall, *High Pressure Research* **14**, 249 (1996).
- [68] H. Träuble, *J. Membr. Biol.* **4**, 193 (1971).
- [69] A. Bakardjieva, H.J. Galla and E.J. Helmreich, *Biochemistry* **76**, 3016 (1979).
- [70] M. Höchli and C.R. Hackenbrock, *Proc. Natl. Acad. Sci. USA* **76**, 1236 (1979).
- [71] W. Pfeiffer, T. Henkel, E. Sackmann, W. Knoll and D. Richter, *Europhys. Lett.* **8**, 201 (1989).
- [72] H. Schindler, and J. Seelig, *Biochemistry* **14**, 2283 (1975).